
Learning Dynamic Graph Representation of Brain Connectome with Spatio-Temporal Attention

Byung-Hoon Kim *
Yonsei University
egyptdj@yonsei.ac.kr

Jong Chul Ye
KAIST
jong.ye@kaist.ac.kr

Jae-Jin Kim
Yonsei University
jaejkim@yonsei.ac.kr

Abstract

Functional connectivity (FC) between regions of the brain can be assessed by the degree of temporal correlation measured with functional neuroimaging modalities. Based on the fact that these connectivities build a network, graph-based approaches for analyzing the brain connectome have provided insights into the functions of the human brain. The development of graph neural networks (GNNs) capable of learning representation from graph structured data has led to increased interest in learning the graph representation of the brain connectome. Although recent attempts to apply GNN to the FC network have shown promising results, there is still a common limitation that they usually do not incorporate the dynamic characteristics of the FC network which fluctuates over time. In addition, a few studies that have attempted to use dynamic FC as an input for the GNN reported a reduction in performance compared to static FC methods, and did not provide temporal explainability. Here, we propose STAGIN, a method for learning *dynamic* graph representation of the brain connectome with spatio-temporal attention. Specifically, a temporal sequence of brain graphs is input to the STAGIN to obtain the dynamic graph representation, while novel READOUT functions and the Transformer encoder provide spatial and temporal explainability with attention, respectively. Experiments on the HCP-Rest and the HCP-Task datasets demonstrate exceptional performance of our proposed method. Analysis of the spatio-temporal attention also provide concurrent interpretation with the neuroscientific knowledge, which further validates our method. Code is available at <https://github.com/egyptdj/stagin>

1 Introduction

Neuroimaging modalities provide measurements of brain activity by capturing the signals of neural activity. Functional magnetic resonance imaging (fMRI) is a non-invasive imaging method that measures the blood-oxygen level dependence (BOLD) in order to estimate the neural activity of the whole brain over time [15]. Functional connectivity (FC) is defined as the degree of temporal correlation between regions of the brain. Based on the fact that these connectivities form networks that change over time, graph-based network analysis of brain connectome has been one of the key approaches to understanding how the brain works [6, 4, 31].

*Work partially performed at KAIST

Graph neural networks (GNNs) are a type of deep neural networks that have recently been successful in learning the representation of graph-structured data [37]. The graph-structured nature of the brain has led to an increased interest in learning the representation of the brain FC network with the GNNs. Learning the representation of the brain connectome has both positive and negative potential social implications, as it can be linked to the search for new biomarkers of a particular phenotype. Accordingly, the current trend in studies attempting to apply GNN to the brain connectome is to input the FC graph from either resting-state [19, 20, 2, 24, 18, 35, 36] or task fMRI data [21–23] and predict a particular phenotype of the subjects, such as gender [20, 2, 18, 17] or presence of a specific disease [20, 24, 21–23, 17]. While these studies have shown potential strengths and opportunities for learning the network representation of the brain, they also suggest limitations of current GNN-based methods.

One of the most common limitations with previous GNN-based FC network analysis methods is that most of them fail to take advantage of the dynamic properties of the FC network, which fluctuates over time. Incorporating the dynamic features of the FC network into the neuroimaging analysis has been an important direction in the field of functional neuroimaging [16, 27]. A work by [11] tried to address this issue by using the Spatial Temporal Graph Convolutional Network (ST-GCN) [40] model to incorporate dynamic features of the FC network. However, [11] reported lower accuracy than other non-dynamic GNN-based FC methods [18, 2] in the gender classification experiment, leaving a question about the effectiveness of the dynamic FC method. In addition, another limitation of the method is that no temporal explainability is provided from the model. This is a major drawback considering that the goal of applying GNNs to functional neuroimaging methods is not only to achieve high classification accuracy, but also to uncover the functional basis of the brain [18, 23]. Another recent work by [3], using GraphNets [5] and DiffPool [43] for the dynamic FC analysis, also suffers from the same limitations in terms of poor classification accuracy and lack of temporal explainability.

Here, we propose Spatio-Temporal Attention Graph Isomorphism Network (STAGIN) for learning the dynamic graph representation of the brain connectome with spatio-temporal attention. The proposed method exploits the temporal features of the dynamic FC network graphs to improve the classification accuracy of the model. In particular, we address the issue that the node features of the input dynamic graph do not contain any temporal information and concatenate encoded timestamp with the node features (Section 3.1). In addition, the proposed method includes novel attention-based READOUT modules (Section 3.2) and the Transformer encoder [34] (Section 3.3) in order to further improve the classification performance and provide spatial-temporal explainability at the same time. STAGIN achieves state-of-the-art performance with the Human Connectome Project (HCP) dataset [33] in gender classification for resting state fMRI and task decoding for task fMRI. We inherit k-means clustering analysis of the resting-state dynamic FC [1] and general linear model (GLM) statistical mapping of task fMRI [10] for interpreting the spatio-temporal attention learned from STAGIN. The interpretation of the learned spatio-temporal attention replicates neuroscientific findings from previous large-scale fMRI studies in both resting-state and task fMRI, which further validates our proposed method. It should also be noted that to the best of our knowledge, this is the first study to demonstrate the capability to learn the dynamic graph representation of both resting-state and task fMRI data with a single framework.

2 Theory

2.1 Problem definition

The goal of our study is to train a neural network

$$f : G_{\text{dyn}} \rightarrow \mathbf{h}_{G_{\text{dyn}}},$$

where $G_{\text{dyn}} = (G(1), \dots, G(T))$ is the sequence of brain graphs with T timepoints and $\mathbf{h}_{G_{\text{dyn}}} \in \mathbb{R}^D$ is the vector representation of the dynamic graph $G(t)$ with length D . The graph $G(t) = (V(t), E(t))$ at time t is a pair of vertex set $V(t) = \{\mathbf{x}_1(t), \dots, \mathbf{x}_N(t)\}$ of N nodes and edge set $E(t) = \{\{\mathbf{x}_i(t), \mathbf{x}_j(t)\} \mid j \in \mathcal{N}(i), i \in \{1, \dots, N\}\}$ where $\mathcal{N}(i)$ denotes the neighborhood of the vertex i . If f learns to extract a disentangled representation of the dynamic brain graph G_{dyn} , then the classification of a certain phenotypic characteristic (e.g. gender) from $\mathbf{h}_{G_{\text{dyn}}}$ can be performed with a linear mapping as a downstream task. Another important consideration in this work is to ensure the explainability of the model f , being able to inform us which part of the brain at which timepoint

was considered important when extracting the meaningful representation $\mathbf{h}_{G_{\text{dyn}}}$. Specifically, we formulate $f = g \circ q$ as a composition of the GNN g and the Transformer encoder q , where g outputs the set of graph representations $\mathbf{h}_{G(t)}$ from each timepoint and q exploits self-attention to integrate $\mathbf{h}_{G(t)}$ into the final representation $\mathbf{h}_{G_{\text{dyn}}}$:

$$g : G_{\text{dyn}} \rightarrow (\mathbf{h}_{G(1)}, \dots, \mathbf{h}_{G(T)}), \quad (1)$$

$$q : (\mathbf{h}_{G(1)}, \dots, \mathbf{h}_{G(T)}) \rightarrow \mathbf{h}_{G_{\text{dyn}}}. \quad (2)$$

We will omit timepoint notation (t) for brevity, whenever it is not of contextual importance.

2.2 Graph Isomorphism Network

The GNNs are generally composed of functions that (i) integrate the node features from its neighbors, and (ii) embed the integrated information with a nonlinear transformation to obtain the next layer node features. These functions are called AGGREGATE, and COMBINE functions, respectively, and the choice of these functions define many variants of the GNN,

$$\mathbf{a}_v^{(k)} = \text{AGGREGATE}^{(k)}\left(\left\{\mathbf{h}_u^{(k-1)} : u \in \mathcal{N}(v)\right\}\right), \quad (3)$$

$$\mathbf{h}_v^{(k)} = \text{COMBINE}^{(k)}\left(\mathbf{h}_v^{(k-1)}, \mathbf{a}_v^{(k)}\right), \quad (4)$$

where $\mathbf{h}_v^{(k)}$ denotes the feature vector of node v at layer k and $\mathbf{h}_v^{(0)} := \mathbf{x}_v$.

The Graph Isomorphism Network (GIN) is a variant of the GNN suitable for graph classification tasks, which is known to be as powerful as the WL-test under certain assumptions of injectivity [38]. The GIN typically defines sum as the AGGREGATE and a multi-layer perceptron (MLP) with two layers as the COMBINE updating the node representation $\mathbf{h}_v^{(k)}$ at layer k [38] by :

$$\mathbf{h}_v^{(k)} = \text{MLP}^{(k)}\left(\left(1 + \epsilon^{(k)}\right) \cdot \mathbf{h}_v^{(k-1)} + \sum_{u \in \mathcal{N}(v)} \mathbf{h}_u^{(k-1)}\right), \quad (5)$$

where ϵ is a learnable parameter initialized with zero. Equation (5) can be easily reformulated into the matrix form [18] by:

$$\mathbf{H}^{(k)} = \sigma\left(\left(\epsilon^{(k)} \cdot \mathbf{I} + \mathbf{A}\right)\mathbf{H}^{(k-1)}\mathbf{W}^{(k)}\right), \quad (6)$$

where

$$\mathbf{H}^{(k)} = \left[\mathbf{h}_1^{(k)}, \dots, \mathbf{h}_N^{(k)}\right] \in \mathbb{R}^{D \times N}$$

is the stack of node feature vectors, \mathbf{I} is the identity matrix, \mathbf{A} is the adjacency matrix between the node features, \mathbf{W} is the network weights of the MLP, and σ is the nonlinearity function.

The READOUT function takes the updated node features $\mathbf{h}_v^{(k)}$ to compute the representation of the whole graph:

$$\mathbf{h}_G^{(k)} = \text{READOUT}\left(\left\{\mathbf{h}_v^{(k)} \mid v \in G\right\}\right). \quad (7)$$

In general, the READOUT function is defined simply as computing the sum or average of the input node features. This is equivalent to multiplication with the length N pooling vectors $\Phi_{\text{sum}}^\top = [1, \dots, 1]$ or $\Phi_{\text{mean}}^\top = [1/N, \dots, 1/N]$ for the matrix form:

$$\mathbf{h}_G^{(k)} = \mathbf{H}^{(k)}\Phi_{\text{mean}}. \quad (8)$$

2.3 Encoder-decoder understanding of GNNs

Although formulating the GIN (5) as a combination of AGGREGATE and COMBINE function might not suggest its close relationship with convolutional neural networks (CNNs) at first glance, previous works by [18, 7] show that the matrix formulation of the GIN operation (6) can be thought of a CNN layer with shift operation of the convolution as the adjacency matrix \mathbf{A} . We extend the understanding

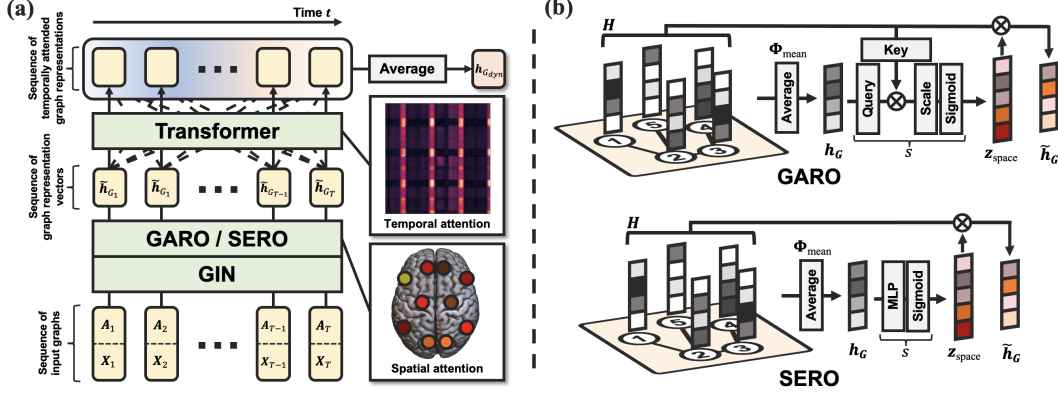


Figure 1: Schematic illustration of the proposed method. (a) Overall framework of the STAGIN. (b) Attention-based READOUT modules.

of encoder-decoder CNN as a framelet expansion [42, 41] to the GIN to formulate node feature vectors $H^{(k)}$ at layer k with respect to the input node feature x_i as:

$$H^{(k)} = \Sigma^{(k)} E^{(k)\top} \dots \Sigma^{(1)} E^{(1)\top} [x_1, \dots, x_N] \quad (9)$$

where the k -th layer encoder matrix $E^{(k)}$ is defined as

$$E^{(k)} = W^{(k)} \otimes (\epsilon^{(k)} \cdot I + A)$$

and $\Sigma^{(k)}$ is the diagonal matrix with values 1 or 0 depending on the activation pattern of the nonlinearity. Now, Φ_{mean} of equation (8) can be thought as the decoder at the k -th layer which yields the whole graph feature vector from the encoded node feature vectors.

Proposition 1. *The READOUT function Φ_{mean} in (8) correspond to a decoder with fixed constant frame bases.*

Proof. Encoder expansion of the GIN (9) can be formulated as

$$h_{i,j}^{(k)} = \langle b_i, x_j \rangle, \quad (10)$$

where the basis b_i of the encoder is given by

$$[b_1, \dots, b_D]^\top = E^{(1)} \Sigma^{(1)} \dots E^{(k)} \Sigma^{(k)},$$

and $x_j, h_{i,j}$ denote the j -th column of X and (i, j) -th element of H , respectively. Decoding the whole graph feature from the encoded node features can be thought of:

$$h_G^{(k)}[i] = \frac{1}{N} \sum_{j=1}^N h_{i,j}^{(k)} = \sum_{j=1}^N \langle b_i, x_j \rangle \tilde{b}_i, \quad (11)$$

where the i -th element of the decoder basis vector $\tilde{b} \in \mathbb{R}^N$ correspond to the constant value $\tilde{b}_i = \frac{1}{N}$ irrespective of the index, suggesting the equality of fixed constant decoder frame basis \tilde{b} and the READOUT function Φ_{mean} . \square

We address the issue that the decoder being a constant function can restrict the expressivity of the neural network, and explore adaptive READOUT functions with attention in Section 3.2.

3 STAGIN: Spatio-Temporal Attention Graph Isomorphism Network

In this section, we discuss the details of our main contribution. Specifically, we propose STAGIN with two novel attention-based READOUT modules for learning the dynamic graph representation of the brain connectome (Figure 1).

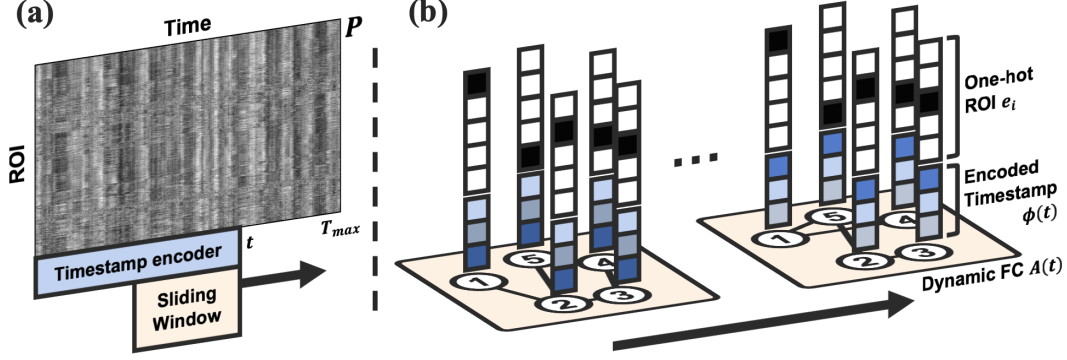


Figure 2: Defining the dynamic graph (a) Scheme of extracting dynamic graph from ROI-timeseries matrix \mathbf{P} (b) Example of a constructed dynamic graph.

3.1 Dynamic graph definition

The sequence of input dynamic FC graphs is constructed from 4D fMRI data with 3D voxels across time. The ROI-timeseries matrix $\mathbf{P} \in \mathbb{R}^{N \times T_{\max}}$ is extracted by taking the mean values within a pre-defined 3D atlas which consists of N ROIs at each timepoint. Values of each ROI are standardized across time. Constructing dynamic FC matrix follows the sliding-window approach, where the temporal window of length Γ is shifted across time with stride S to generate $T = \lfloor T_{\max} - \Gamma/S \rfloor$ windowed matrices $\bar{\mathbf{P}}(t) \in \mathbb{R}^{N \times \Gamma}$ (Figure 2 (a)). The FC at time t is defined as the correlation coefficient matrix $\mathbf{R}(t)$ of the windowed timeseries between $\bar{\mathbf{p}}_i(t)$ and $\bar{\mathbf{p}}_j(t)$:

$$R_{ij}(t) = \frac{\text{Cov}(\bar{\mathbf{p}}_i(t), \bar{\mathbf{p}}_j(t))}{\sigma_{\bar{\mathbf{p}}_i(t)} \sigma_{\bar{\mathbf{p}}_j(t)}} \in \mathbb{R}^{N \times N},$$

where the subscript i and j are the row and column indices of $\bar{\mathbf{P}}(t)$, Cov denotes the cross covariance, and $\sigma_{\mathbf{p}}$ denotes the standard deviation of \mathbf{p} . The final binary adjacency matrix $\mathbf{A}(t) \in \{0, 1\}^{N \times N}$ is obtained from the FC matrix $\mathbf{R}(t)$ by thresholding the top 30-percentile values of the correlation matrix as connected, and otherwise unconnected following [18].

Unlike the adjacency matrix $\mathbf{A}(t)$, conventional definition of node feature vectors $\mathbf{x}_i(t)$ as coordinates [21], mean-activation [21, 11], or one-hot encoding [18], do not change over t , disregarding any temporal variation. To address this issue, we concatenate encoded timestamp $\phi(t) \in \mathbb{R}^D$ to the spatial one-hot encoding \mathbf{e}_v , followed by linear mapping with a learnable parameter matrix $\mathbf{W} \in \mathbb{R}^{D \times (N+D)}$ to define the input node feature,

$$\mathbf{x}_v(t) = \mathbf{W}[\mathbf{e}_v || \phi(t)]. \quad (12)$$

Here, the learnable timestamp encoder ϕ is a Gated Recurrent Unit (GRU) [8] which takes ROI-timeseries upto the endpoint of the sliding-window as the input. Both the vertex set $V(t)$ and the edge set $E(t)$ of graph $G(t)$ now incorporates temporal information at time t . See Figure 2 for an illustration of the dynamic graph definition.

3.2 Spatial attention with attention-based READOUT

As suggested from Proposition 1, conventional READOUT function of GNN can be thought of as a fixed decoder that decodes whole-graph feature from the node features with no learnable parameters. We address this issue by incorporating attention to the READOUT function, which the attention here refers to the scaling coefficient across the nodes learned by the model. Specifically, the spatial attention vector $\mathbf{z}_{\text{space}}(t) \in [0, 1]^N$ is computed by taking the \mathbf{H} as a prior:

$$\mathbf{z}_{\text{space}} = s(\mathbf{H}), \quad (13)$$

$$\tilde{\mathbf{h}}_G = \mathbf{H} \mathbf{z}_{\text{space}}, \quad (14)$$

where $s : \mathbb{R}^{D \times N} \rightarrow [0, 1]^N$ is the attention function and $\tilde{\mathbf{h}}_G$ denotes spatially attended graph representation \mathbf{h}_G . We propose two types of attention function $s(\cdot)$ for the attention-based READOUT, named Graph-Attention READOUT (GARO) and Squeeze-Excitation READOUT (SERO) inspired by the attention mechanisms of [34] and [14], respectively.

3.2.1 GARO: Graph-Attention READOUT

The GARO follows key-query embedding based attention of the Transformer [34]. However, the key embedding is computed from the matrix of node features \mathbf{H} , while the query embedding is computed from the vector of unattended graph representation $\mathbf{H}\Phi_{\text{mean}}$:

$$\begin{aligned} \mathbf{K} &= \mathbf{W}_{\text{key}}\mathbf{H}, \\ \mathbf{q} &= \mathbf{W}_{\text{query}}\mathbf{H}\Phi_{\text{mean}}, \\ \mathbf{z}_{\text{space}} &= \text{sigmoid}\left(\frac{\mathbf{q}^\top \mathbf{K}}{\sqrt{D}}\right), \end{aligned} \quad (15)$$

where $\mathbf{W}_{\text{key}} \in \mathbb{R}^{D \times D}$, $\mathbf{W}_{\text{query}} \in \mathbb{R}^{D \times D}$ are learnable key-query parameter matrices, $\mathbf{K} \in \mathbb{R}^{D \times N}$ is the embedded key matrix, and $\mathbf{q} \in \mathbb{R}^D$ is the embedded query vector.

3.2.2 SERO: Squeeze-Excitation READOUT

The SERO follows MLP based attention of the Squeeze-and-Excitation Networks [14]. However, attention from the *squeezed* graph representation does not scale the channel dimension, but the node dimension in SERO:

$$\mathbf{z}_{\text{space}} = \text{sigmoid}\left(\mathbf{W}_2 \sigma(\mathbf{W}_1 \mathbf{H} \Phi_{\text{mean}})\right), \quad (16)$$

where σ is the nonlinearity function and $\mathbf{W}_1 \in \mathbb{R}^{D \times D}$, $\mathbf{W}_2 \in \mathbb{R}^{N \times D}$ are learnable parameter matrices. This type of spatial dimension squeeze-excitation module has been shown to improve performance of the CNN models [29], but was not easily applicable to general graphs which may vary in number of nodes for each graph. We exploit the fact that the brain graphs have fixed number of nodes N across participants based on the chosen atlas.

3.2.3 Orthogonal regularization

If we take a closer look at (8) and (14), computation of graph feature vector \mathbf{h}_G from the node feature matrix \mathbf{H} can also be viewed as reconstructing signal \mathbf{h}_G from the basis frames \mathbf{H} with coefficient vectors Φ_{mean} and $\mathbf{z}_{\text{space}}$, respectively. While $\mathbf{z}_{\text{space}}$ provides further expressivity of the model with adaptive coefficients when compared to Φ_{mean} , we find it desirable to encourage the orthogonality of \mathbf{H} . The orthogonal regularization $\mathcal{L}_{\text{ortho}}$ is defined as:

$$\mathcal{L}_{\text{ortho}} = \left\| \frac{1}{m} \cdot \mathbf{H}^\top \mathbf{H} - \mathbf{I} \right\|_2, \quad (17)$$

where $m = \max(\mathbf{H}^\top \mathbf{H})$. The scaling term $1/m$ ensures the columns of the matrix \mathbf{H} become orthogonal to each other with the same length, while not restricting the specific length that the column vectors should follow.

3.3 Temporal attention with Transformer encoder

For attention across time, we employ a single-headed Transformer encoder [34] upon the sequence of graph features $(\tilde{\mathbf{h}}_{G(1)}, \dots, \tilde{\mathbf{h}}_{G(T)})$. The temporal attention can be measured by the self-attention weights $\mathbf{Z}_{\text{time}} \in [0, 1]^{T \times T}$ after the softmax function of the Transformer encoder. Per-layer dynamic graph representation $\mathbf{h}_{G_{\text{dyn}}}^{(k)}$ is computed by summing the temporally attended feature output from the Transformer encoder across time at each layers, where the final representation:

$$\mathbf{h}_{G_{\text{dyn}}} = \text{concatenate}(\{\mathbf{h}_{G_{\text{dyn}}}^{(k)} \mid k \in \{1, \dots, K\}\}) \quad (18)$$

is the concatenation of dynamic graph representation of all K layers following [39].

4 Experiment

4.1 Dataset

Publicly available² fMRI data from the HCP S1200 release [33] was used for our experiments. The data was collected from voluntary participants with informed consent and was fully anonymized.

²<https://db.humanconnectome.org>

Table 1: Comparative study on HCP-Rest and HCP-Task dataset. N/A is short for Not Applicable.

Model	HCP-Rest		HCP-Task
	Accuracy (%)	AUROC	Accuracy (%)
STAGIN-SERO	88.20 \pm 1.33	0.9296 \pm 0.0187	99.19 \pm 0.20
STAGIN-GARO	87.01 \pm 3.00	0.9151 \pm 0.0258	99.02 \pm 0.17
ST-GCN [11]	76.95 \pm 3.00	0.8545 \pm 0.0316	N/A
BAnD++ [26]		N/A	97.20 \pm 0.57
BAnD [26]		N/A	95.10 \pm 0.62

We constructed two datasets, the HCP-Rest and the HCP-Task, depending on whether the subject was resting or performing specific tasks during the acquisition of the image. The HCP-Rest dataset consisted of pre-processed and ICA denoised resting-state fMRI data [12], which the subjects were instructed to rest for 15 minutes during the data acquisition. We used first run data of the four sessions, and excluded data with short acquisition time with $T_{\max} < 1200$. There were 1093 images finally included in the dataset, which consisted of 594 female and 499 male subjects. The gender of each subject served as the labels of the HCP-Rest dataset letting the number of classes $C = 2$. The HCP-Task consisted of pre-processed task fMRI data [12], which the subjects were instructed to perform specific tasks during data acquisition. For example in the "Motor" task fMRI, participants were told to perform one of the subtasks during the acquisition to make motor movements on the left hand, left foot, right hand, right foot, or tongue. There were seven types of tasks including working memory, social, relational, motor, language, gambling, and emotion. After excluding the fMRI data with short acquisition time, there were 7450 images included in the dataset. The task type during the data acquisition served as the labels of the HCP-Task dataset, letting $C = 7$. A summary of the experiment datasets can be found in Table 2 in the Appendix.

4.2 Experimental settings

Experiments were performed on a workstation with two NVIDIA GeForce GTX 1080 Ti GPUs. The STAGIN model f is trained end-to-end in a supervised manner with the loss $\mathcal{L} = \mathcal{L}_{\text{xent}} + \lambda \cdot \mathcal{L}_{\text{ortho}}$ where $\mathcal{L}_{\text{xent}}$ is the cross entropy loss and λ is the scaling coefficient of the orthogonal regularization. We set the number of layers $K = 4$, embedding dimension $D = 128$, window length $\Gamma = 50$, window stride $S = 3$, and regularization coefficient $\lambda = 1.0 \times 10^{-5}$. The window length and stride correspond to capturing the FC within 36 seconds every 2.16 seconds, which follows the standard setting of the sliding-window dFC analyses [44, 27]. Dropout rate 0.5 is applied to the final dynamic graph representation $h_{G_{\text{dyn}}}$, and rate 0.1 is applied to the attention vectors z_{space} and z_{time} during training. For nonlinearity σ in (6) and (16), GELU [13] is used instead of ReLU with batch normalization before each σ . One-cycle learning rate policy is employed, which the learning rate is gradually increased from 0.0005 to 0.001 during the early 20% of the training, and gradually decreased to 5.0×10^{-7} afterwards. Thirty training epochs were run for the HCP-Rest dataset with minibatch size 3, while ten epochs were run with minibatch size 16 for the HCP-Task dataset. We performed 5-fold stratified cross-validation of the dynamic graphs from the dataset, and report mean and standard deviation across the folds. To extract the ROI-timeseries, the Schaefer atlas [30] with 400 regions ($N = 400$) labelled with 7 intrinsic connectivity networks (ICNs) was used. The time dimension of ROI-timeseries matrix P was randomly sliced with a fixed length (600 for HCP-Rest, 150 for HCP-Task) at each steps during training for (i) mitigating computational overload, (ii) stochastic augmentation of the training dataset, and (iii) matching the number of timepoints T across different task labels for the HCP-Task dataset. Unsliced full matrix P was used for inference at test time.

4.3 HCP-Rest: Gender classification

We first validate our proposed method by gender classification on the HCP-Rest dataset. The two proposed methods, named STAGIN-GARO and STAGIN-SERO based on the type of the spatial attention module, resulted in 87.01% and 88.20% mean accuracy on the 5-fold cross validation, respectively (Table 1). The mean area under receiver operator characteristic curve (AUROC) were 0.9151 and 0.9296. The classification performance of STAGIN is compared with the previous state-of-the-art GNN method for representation learning of dynamic FC network by [11], which employed

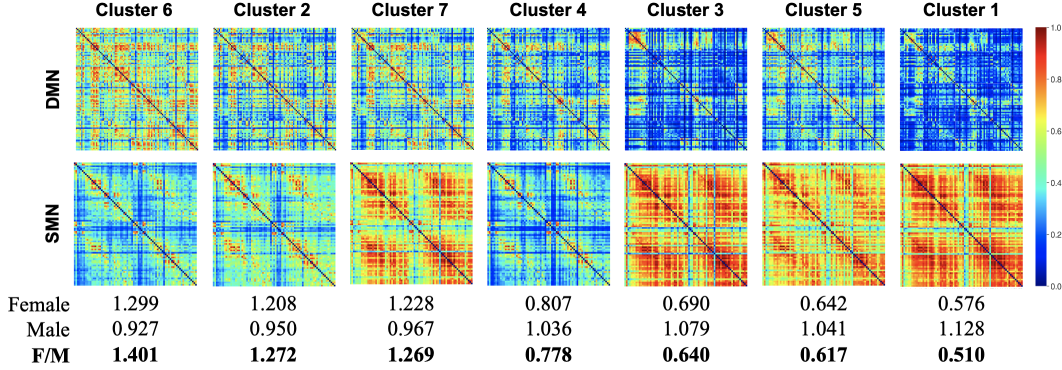


Figure 3: Analysis of temporal attention of the gender classification experiment with k-means clustering. The DMN and SMN of the 7 cluster centroids are plotted and the relative proportion of temporally attended clusters for female and male subjects are written below. The clusters are sorted in descending order of the female/male attended cluster ratio.

ST-GCN to the HCP-Rest dataset for gender classification. We used the code by the authors³ of [11] but modified the cross validation scheme to avoid early stopping based on the test dataset for fair comparison. The ST-GCN resulted in 76.95% accuracy and 0.8545 AUROC for gender classification on the HCP-Rest dataset. The results of the ablation study are shown in Table 3 in the Appendix.

We use STAGIN-SERO, which showed the best accuracy, for analyzing temporal and spatial attention of the dynamic FC networks. We define the temporal attention vector $\mathbf{z}_{\text{time}}^{(k)} \in [0, 1]^T$ at layer k as the average of columns in the self-attention weight matrix $\mathbf{z}_{\text{time}}^{(k)} = \frac{1}{T} \sum_{i=1}^T Z_{ij}$ where Z_{ij} is the (i, j) -th element of $\mathbf{Z}_{\text{time}}^{(k)}$ for the resting-state data. To employ k-means clustering to the resting-state dynamic FC analysis [1], we first define a set of *attended* timepoints $\tilde{T} = \{t \mid \mathbf{z}_{\text{time}}[t] > \alpha \cdot \sigma_{\mathbf{z}_{\text{time}}}\}$ where α is the cutoff coefficient, and $\sigma_{\mathbf{z}_{\text{time}}}$ denotes the standard deviation of $\mathbf{z}_{\text{time}}^{(k)}$. Defining the threshold based on standard deviation inherits the practice of the point-process analysis for dynamic FC, so we set $\alpha = 1.0$ following [32]. Pattern of the FC matrices at attended timepoints $\mathbf{A}^{\tilde{T}} = \{\mathbf{A}(t) \mid t \in \tilde{T}\}$ for each subject can now be analyzed with the k-means clustering. Specifically, we fit 7 template cluster centroids from the dynamic FC matrices $\mathbf{A}(t)$ over all subjects, and assign elements of $\mathbf{A}^{\tilde{T}}$ into one of the 7 template clusters. The ratio of each clusters from $\mathbf{A}^{\tilde{T}}$ with respect to \mathbf{A} can then be analyzed with the subset of $\mathbf{A}^{\tilde{T}}$ including only the female or male subjects.

Evidences from large scale studies suggest that female subjects show hyperconnectivity of the DMN [25, 28] and hypoconnectivity of the SMN when compared to male subjects [28, 9]. We accordingly hypothesized that the FC at attended timepoints will show higher values for the DMN and lower values for the SMN in female participants. Figure 3 demonstrates that the clusters mainly attended by female participants show a trend of hyperconnectivity of the DMN and hypoconnectivity of the SMN. This can be interpreted to mean that the STAGIN is properly trained to take the dynamic state of the FC networks into account for predicting the phenotype of the subject.

The spatial attention across regions of the brain is analyzed with the $\mathbf{z}_{\text{space}}^{(k)}$ averaged across time $\tilde{\mathbf{z}}_{\text{space}}^{(k)} := \frac{1}{T} \sum_{t=1}^T \mathbf{z}_{\text{space}}^{(k)}(t)$. The regions with top 5 percentile attention values of $\tilde{\mathbf{z}}_{\text{space}}^{(k)}$ are plotted with respect to the seven ICNs in Figure 8 in the Appendix. It can be seen that the majority of the top attended regions are from the SMN, which further suggests gender difference of resting-state FC within the SMN. A notable limitation here is that the threshold for determining the top attended region is heuristically set. Statistically determining the spatially attended regions from the resting-state data would further provide validity of the method, which is left as a future work.

³https://github.com/sgadgil6/cnslab_fmri

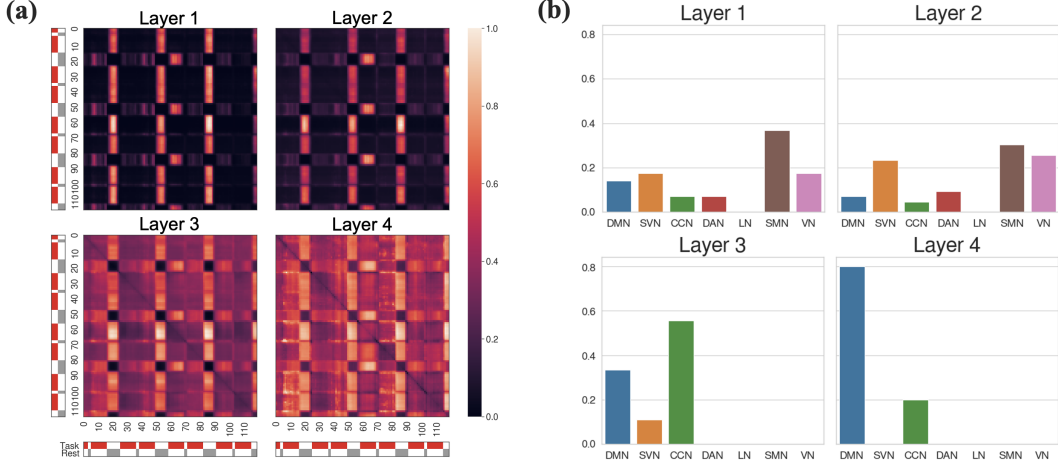


Figure 4: Analysis of spatio-temporal attention for working memory task of the task decoding experiment. (a) Plot of average temporal attention matrix $Z_{\text{time}}^{(k)}$ across subjects. (b) Proportion of statistically significant regions within the 7 ICNs from the spatial attention GLM.

4.4 HCP-Task: Task decoding

Task decoding refers to classifying which of the seven tasks the subject was performing during the acquisition of the brain fMRI. The STAGIN-GARO and STAGIN-SERO showed 99.02% and 99.19% mean accuracy for the task decoding experiment, respectively (Table 1). It can be seen that the proposed methods outperform the previous state-of-the-art model BAND and BAN++ [26], which applied self-attention of the Transformer encoder directly to 3D ResNet extracted representation vectors of the fMRI without considering the network property of the brain.

We interpret the result from the working memory task for spatio-temporal attention analysis, where the subtask consists of either performing an n-back memory task or rest. Our key expectation of the temporal attention analysis was that if STAGIN learns to accurately attend to temporal features of the dynamic FC graphs, then Z_{time} should represent which subtask the subject was upto. Surprisingly, it can be clearly seen that the Transformer encoder of STAGIN learns to attend to the timing of subtasks from Figure 4 (a), which demonstrates mean temporal attention Z_{time} across all subjects. Notice that no supervision is provided to the STAGIN model regarding the subtask timing during training.

To analyze the spatially attended regions z_{space} of STAGIN, we construct a GLM [10] to statistically evaluate how much each region is responsible for performing the subtasks. The parameter vectors $\beta_{\text{task}} \in \mathbb{R}^N$ and $\beta_{\text{rest}} \in \mathbb{R}^N$ are estimated with the sequence of spatial attention vectors and the subtask timing design matrix $M \in \{0, 1\}^{T \times 2}$ by solving the following with least-squares estimation:

$$[z_{\text{space}}(0), \dots, z_{\text{space}}(T)]^T = M[\beta_{\text{task}}, \beta_{\text{rest}}]^T + \epsilon,$$

where ϵ denotes residual error. The contrast of the estimated parameters $\hat{\beta}_{\text{task}}$ and $\hat{\beta}_{\text{rest}}$ was set to $c = [1, -1]$ so the rejection of null hypothesis indicates $\hat{\beta}_{\text{task}}[i] > \hat{\beta}_{\text{rest}}[i]$ at the i -th ROI. Multiple comparisons of the N ROIs are family-wise error (FWE) corrected.

Figure 4 (b) shows the proportion of statistically significant regions within the 7 ICNs for each layers. Interestingly, the layer 1 and 2 share a similar trend that the regions from SMN, visual network (VN), and salience/ventral attention network (SVN) are dominant. In contrast, layer 3 and 4 suggest a dominance of the regions from DMN and cognitive control network (CCN). We denote the layer 1 and 2 as the low-order layers (LoL) and the layer 3 and 4 as the high-order layers (HoL). The dominance of SMN and VN at LoL can be understood as the low-level sensorimotor function for perceiving the task is being processed within the short-range 1- or 2-hop connection of the networks. On the other hand, the dominance of DMN and CCN at HoL reflects the high-level cognitive integration for executing and controlling the given task being processed within the long-range 3- or 4-hop connection of the networks. Considering that the SVN is a network for integrating the low-level sensorimotor networks and the high-level executive networks to provide dynamic balancing between the two functions, the significant regions of SVN being present at both LoL and HoL is not surprising.

5 Conclusion

We propose STAGIN, a framework for learning dynamic graph representation of brain connectome with spatio-temporal attention which is generally applicable to resting-state and task fMRI data. Experimental results show that STAGIN achieves state-of-the-art performance in gender classification with the HCP-Rest and task decoding with the HCP-Task dataset. Analysis of the spatio-temporal attention learned by STAGIN suggests that the model is capable of providing explainability of the input brain connectome both spatially and temporally.

References

- [1] Elena A Allen, Eswar Damaraju, Sergey M Plis, Erik B Erhardt, Tom Eichele, and Vince D Calhoun. Tracking whole-brain connectivity dynamics in the resting state. *Cerebral cortex*, 24(3):663–676, 2014.
- [2] Salim Arslan, Sofia Ira Ktena, Ben Glocker, and Daniel Rueckert. Graph saliency maps through spectral convolutional networks: Application to sex classification with brain connectivity. In *Graphs in Biomedical Image Analysis and Integrating Medical Imaging and Non-Imaging Modalities*, pages 3–13. Springer, 2018.
- [3] Tiago Azevedo, Alexander Campbell, Rafael Romero-Garcia, Luca Passamonti, Richard AI Bethlehem, Pietro Lio, and Nicola Toschi. A deep graph neural network architecture for modelling spatio-temporal dynamics in resting-stating functional mri data. *bioRxiv*, 2020.
- [4] Danielle S Bassett and Olaf Sporns. Network neuroscience. *Nature neuroscience*, 20(3):353, 2017.
- [5] Peter W Battaglia, Jessica B Hamrick, Victor Bapst, Alvaro Sanchez-Gonzalez, Vinicius Zambaldi, Mateusz Malinowski, Andrea Tacchetti, David Raposo, Adam Santoro, Ryan Faulkner, et al. Relational inductive biases, deep learning, and graph networks. *arXiv preprint arXiv:1806.01261*, 2018.
- [6] Ed Bullmore and Olaf Sporns. Complex brain networks: graph theoretical analysis of structural and functional systems. *Nature reviews neuroscience*, 10(3):186–198, 2009.
- [7] Mark Cheung, John Shi, Oren Wright, Lavendar Y Jiang, Xujin Liu, and José MF Moura. Graph signal processing and deep learning: Convolution, pooling, and topology. *IEEE Signal Processing Magazine*, 37(6):139–149, 2020.
- [8] Junyoung Chung, Caglar Gulcehre, KyungHyun Cho, and Yoshua Bengio. Empirical evaluation of gated recurrent neural networks on sequence modeling. *arXiv preprint arXiv:1412.3555*, 2014.
- [9] Massimo Filippi, Paola Valsasina, Paolo Misci, Andrea Falini, Giancarlo Comi, and Maria A Rocca. The organization of intrinsic brain activity differs between genders: A resting-state fmri study in a large cohort of young healthy subjects. *Human brain mapping*, 34(6):1330–1343, 2013.
- [10] Karl J Friston, Andrew P Holmes, Keith J Worsley, J-P Poline, Chris D Frith, and Richard SJ Frackowiak. Statistical parametric maps in functional imaging: a general linear approach. *Human brain mapping*, 2(4):189–210, 1994.
- [11] Soham Gadgil, Qingyu Zhao, Adolf Pfefferbaum, Edith V Sullivan, Ehsan Adeli, and Kilian M Pohl. Spatio-temporal graph convolution for resting-state fmri analysis. In *International Conference on Medical Image Computing and Computer-Assisted Intervention*, pages 528–538. Springer, 2020.
- [12] Matthew F Glasser, Stamatiou N Sotiropoulos, J Anthony Wilson, Timothy S Coalson, Bruce Fischl, Jesper L Andersson, Junqian Xu, Saad Jbabdi, Matthew Webster, Jonathan R Polimeni, et al. The minimal preprocessing pipelines for the human connectome project. *Neuroimage*, 80:105–124, 2013.
- [13] Dan Hendrycks and Kevin Gimpel. Gaussian error linear units (gelus). *arXiv preprint arXiv:1606.08415*, 2016.
- [14] Jie Hu, Li Shen, and Gang Sun. Squeeze-and-excitation networks. In *Proceedings of the IEEE conference on computer vision and pattern recognition*, pages 7132–7141, 2018.
- [15] Scott A Huettel, Allen W Song, and Gregory McCarthy. *Functional magnetic resonance imaging*, volume 1. Sinauer Associates Sunderland, MA, 2004.
- [16] R Matthew Hutchison, Thilo Womelsdorf, Elena A Allen, Peter A Bandettini, Vince D Calhoun, Maurizio Corbetta, Stefania Della Penna, Jeff H Duyn, Gary H Glover, Javier Gonzalez-Castillo, et al. Dynamic functional connectivity: promise, issues, and interpretations. *Neuroimage*, 80:360–378, 2013.
- [17] Anees Kazi, Soroush Farghadani, and Nassir Navab. Ia-gcn: Interpretable attention based graph convolutional network for disease prediction. *arXiv preprint arXiv:2103.15587*, 2021.
- [18] Byung-Hoon Kim and Jong Chul Ye. Understanding graph isomorphism network for rs-fmri functional connectivity analysis. *Frontiers in neuroscience*, 14:630, 2020.
- [19] Sofia Ira Ktena, Sarah Parisot, Enzo Ferrante, Martin Rajchl, Matthew Lee, Ben Glocker, and Daniel Rueckert. Distance metric learning using graph convolutional networks: Application to functional brain networks. In *International Conference on Medical Image Computing and Computer-Assisted Intervention*, pages 469–477. Springer, 2017.

- [20] Sofia Ira Ktena, Sarah Parisot, Enzo Ferrante, Martin Rajchl, Matthew Lee, Ben Glocker, and Daniel Rueckert. Metric learning with spectral graph convolutions on brain connectivity networks. *NeuroImage*, 169:431–442, 2018.
- [21] Xiaoxiao Li, Nicha C Dvornek, Yuan Zhou, Juntang Zhuang, Pamela Ventola, and James S Duncan. Graph neural network for interpreting task-fMRI biomarkers. In *International Conference on Medical Image Computing and Computer-Assisted Intervention*, pages 485–493. Springer, 2019.
- [22] Xiaoxiao Li, Nicha C Dvornek, Juntang Zhuang, Pamela Ventola, and James Duncana. Graph embedding using infomax for ASD classification and brain functional difference detection. *arXiv preprint arXiv:1908.04769*, 2019.
- [23] Xiaoxiao Li, Yuan Zhou, Siyuan Gao, Nicha Dvornek, Muhan Zhang, Juntang Zhuang, Shi Gu, Dustin Scheinost, Lawrence Staib, Pamela Ventola, et al. BrainGNN: Interpretable brain graph neural network for fMRI analysis. *bioRxiv*, 2020.
- [24] Guixiang Ma, Nesreen K Ahmed, Ted Willke, Dipanjan Sengupta, Michael W Cole, Nick Turk-Browne, and Philip S Yu. Similarity learning with higher-order proximity for brain network analysis. *arXiv preprint arXiv:1811.02662*, 2018.
- [25] Lauren E Mak, Luciano Minuzzi, Glenda MacQueen, Geoffrey Hall, Sidney H Kennedy, and Roumen Milev. The default mode network in healthy individuals: a systematic review and meta-analysis. *Brain connectivity*, 7(1):25–33, 2017.
- [26] Sam Nguyen, Brenda Ng, Alan K Kaplan, and Priyadip Ray. Attend and decode: 4d fMRI task state decoding using attention models. *arXiv preprint arXiv:2004.05234*, 2020.
- [27] Maria Giulia Preti, Thomas AW Bolton, and Dimitri Van De Ville. The dynamic functional connectome: State-of-the-art and perspectives. *Neuroimage*, 160:41–54, 2017.
- [28] Stuart J Ritchie, Simon R Cox, Xueyi Shen, Michael V Lombardo, Lianne M Reus, Clara Alloza, Mathew A Harris, Helen L Alderson, Stuart Hunter, Emma Neilson, et al. Sex differences in the adult human brain: evidence from 5216 UK Biobank participants. *Cerebral Cortex*, 28(8):2959–2975, 2018.
- [29] Abhijit Guha Roy, Nassir Navab, and Christian Wachinger. Recalibrating fully convolutional networks with spatial and channel “squeeze and excitation” blocks. *IEEE transactions on medical imaging*, 38(2):540–549, 2018.
- [30] Alexander Schaefer, Ru Kong, Evan M Gordon, Timothy O Laumann, Xi-Nian Zuo, Avram J Holmes, Simon B Eickhoff, and BT Thomas Yeo. Local-global parcellation of the human cerebral cortex from intrinsic functional connectivity MRI. *Cerebral Cortex*, 28(9):3095–3114, 2017.
- [31] Olaf Sporns. Graph theory methods: applications in brain networks. *Dialogues in clinical neuroscience*, 20(2):111, 2018.
- [32] Enzo Tagliazucchi, Pablo Balenzuela, Daniel Fraiman, and Dante R Chialvo. Criticality in large-scale brain fMRI dynamics unveiled by a novel point process analysis. *Frontiers in physiology*, 3:15, 2012.
- [33] David C Van Essen, Stephen M Smith, Deanna M Barch, Timothy EJ Behrens, Essa Yacoub, Kamil Ugurbil, Wu-Minn HCP Consortium, et al. The Wu-Minn human connectome project: an overview. *Neuroimage*, 80:62–79, 2013.
- [34] Ashish Vaswani, Noam Shazeer, Niki Parmar, Jakob Uszkoreit, Llion Jones, Aidan N Gomez, Łukasz Kaiser, and Illia Polosukhin. Attention is all you need. In *Advances in neural information processing systems*, pages 5998–6008, 2017.
- [35] Simon Wein, WM Malloni, Ana Maria Tomé, Sebastian M Frank, G-I Henze, Stefan Wüst, Mark W Greenlee, and Elmar W Lang. A graph neural network framework for causal inference in brain networks. *Scientific reports*, 11(1):1–18, 2021.
- [36] Dongya Wu, Xin Li, and Jun Feng. Connectome-based individual prediction of cognitive behaviors via the graph propagation network reveals directed brain network topology. *bioRxiv*, 2021.
- [37] Zonghan Wu, Shirui Pan, Fengwen Chen, Guodong Long, Chengqi Zhang, and S Yu Philip. A comprehensive survey on graph neural networks. *IEEE transactions on neural networks and learning systems*, 2020.
- [38] Keyulu Xu, Weihua Hu, Jure Leskovec, and Stefanie Jegelka. How powerful are graph neural networks? *arXiv preprint arXiv:1810.00826*, 2018.

- [39] Keyulu Xu, Chengtao Li, Yonglong Tian, Tomohiro Sonobe, Ken-ichi Kawarabayashi, and Stefanie Jegelka. Representation learning on graphs with jumping knowledge networks. *arXiv preprint [arXiv:1806.03536](https://arxiv.org/abs/1806.03536)*, 2018.
- [40] Sijie Yan, Yuanjun Xiong, and Dahua Lin. Spatial temporal graph convolutional networks for skeleton-based action recognition. In *Proceedings of the AAAI conference on artificial intelligence*, volume 32, 2018.
- [41] Jong Chul Ye, Yoseob Han, and Eunju Cha. Deep convolutional framelets: A general deep learning framework for inverse problems. *SIAM Journal on Imaging Sciences*, 11(2):991–1048, 2018.
- [42] Jong Chul Ye and Woon Kyoung Sung. Understanding geometry of encoder-decoder CNNs. In *International Conference on Machine Learning*, pages 7064–7073, 2019.
- [43] Zhitao Ying, Jiaxuan You, Christopher Morris, Xiang Ren, Will Hamilton, and Jure Leskovec. Hierarchical graph representation learning with differentiable pooling. In *Advances in neural information processing systems*, pages 4800–4810, 2018.
- [44] Andrew Zalesky and Michael Breakspear. Towards a statistical test for functional connectivity dynamics. *Neuroimage*, 114:466–470, 2015.

Appendix

Table 2: Summary of the experiment datasets

Dataset	Task type	Subtasks	No. images	T_{\max}	C
HCP-Rest	Resting-state	Rest	1093	1200	2
	Working Memory	Task, Rest	1087	405	
HCP-Task	Social	Mental, Random, Rest	1053	274	
	Relational	Task, Rest	1043	232	
	Motor	(L,R).(Hand,Foot), Tongue, Rest	1085	284	7
	Language	Story, Math, Response	1051	316	
	Gambling	Task, Rest	1082	253	
	Emotion	Shape, Face, Rest	1049	176	

Table 3: Ablation study

Atlas	N	$\mathcal{L}_{\text{ortho}}$	z_{space}	Z_{time}	$\phi(t)$	Accuracy (%)	AUROC
Schaefer	400	✓	✓	✓	✓	88.20 ± 1.33	0.9296 ± 0.0187
		✗	✓	✓	✓	87.46 ± 3.56	0.9213 ± 0.0242
		✗	✗	✓	✓	86.55 ± 3.12	0.9260 ± 0.0216
		✗	✗	✗	✓	85.64 ± 2.47	0.9272 ± 0.0104
		✗	✗	✗	✗	82.34 ± 3.38	0.9005 ± 0.0256
AAL	116	✓	✓	✓	✓	85.36 ± 1.58	0.9216 ± 0.0116
Destrieux	150	✓	✓	✓	✓	85.73 ± 1.39	0.9235 ± 0.0126
Harvard-oxford	48	✓	✓	✓	✓	82.07 ± 1.11	0.9008 ± 0.0093

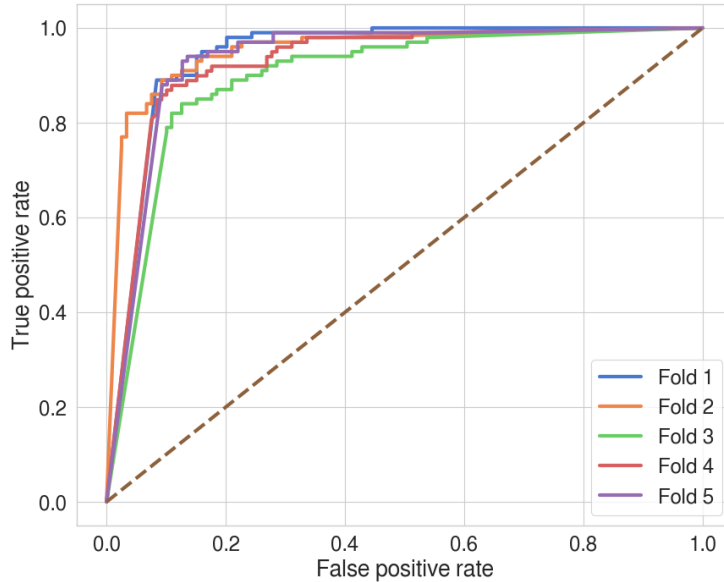


Figure 5: Receiver operating characteristic curve of STAGIN-SERO for the HCP-Rest test data.

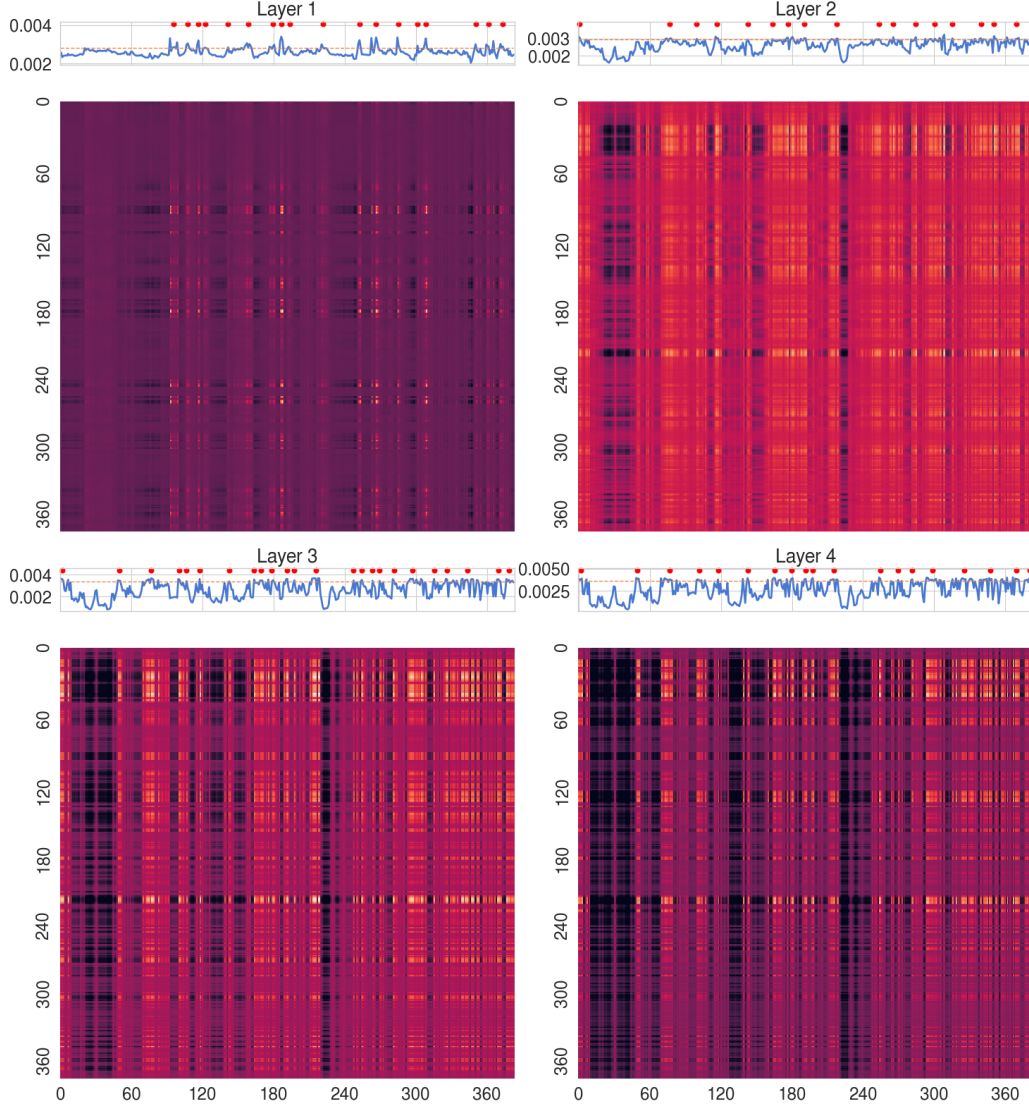


Figure 6: Exemplar plot of the resting-state temporal attention $Z_{\text{time}}^{(k)}$ of a random test subject. Lineplot of the column averaged temporal attention $z_{\text{time}}^{(k)}$ is shown above each matrix plots. Orange dotted lines denote the cutoff value and the red dots represent elements of the attended timepoints A^T .

We find that non-informative attention signal is carried along the queries of $Z_{\text{time}}^{(k)}$. Thus, we define the temporal attention vector $z_{\text{time}}^{(k)} \in [0, 1]^T$ at layer k as the average of columns in the self-attention weight matrix $z_{\text{time}}^{(k)} = \frac{1}{T} \sum_{i=1}^T Z_{ij}$ where Z_{ij} is the (i, j) -th element of $Z_{\text{time}}^{(k)}$ for the resting-state data (see Section 4.3).

Also, to reduce redundancy of the attended timepoints A^T , we only consider one element from the consecutive timepoints. The element is selected from the center index (red dots of Figure 6).

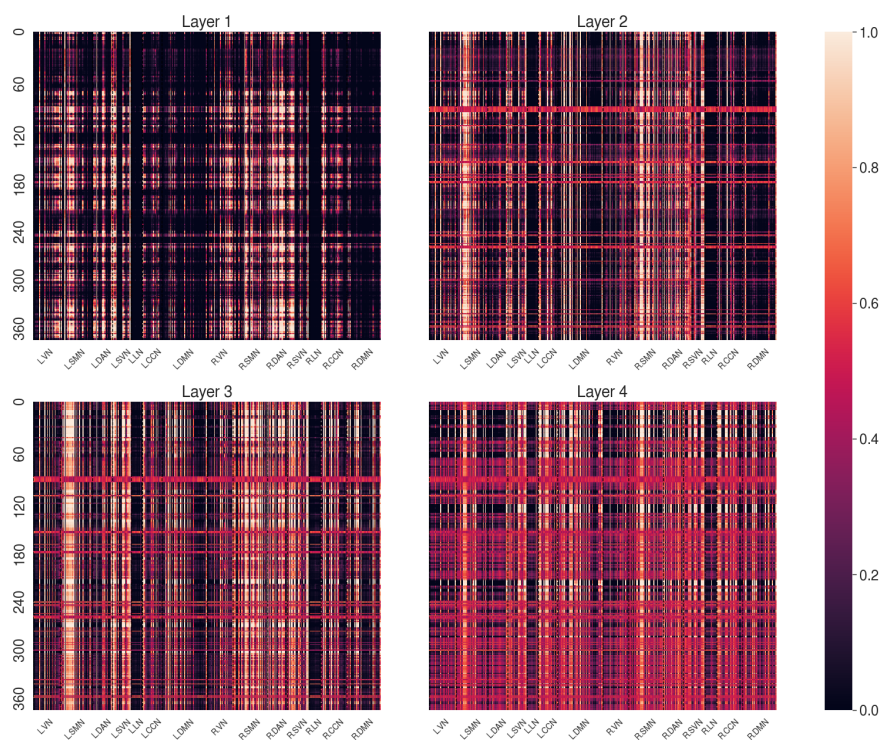


Figure 7: Exemplar plot of the resting-state spatial attention $z_{\text{space}}^{(k)}(t)$ of a random test subject

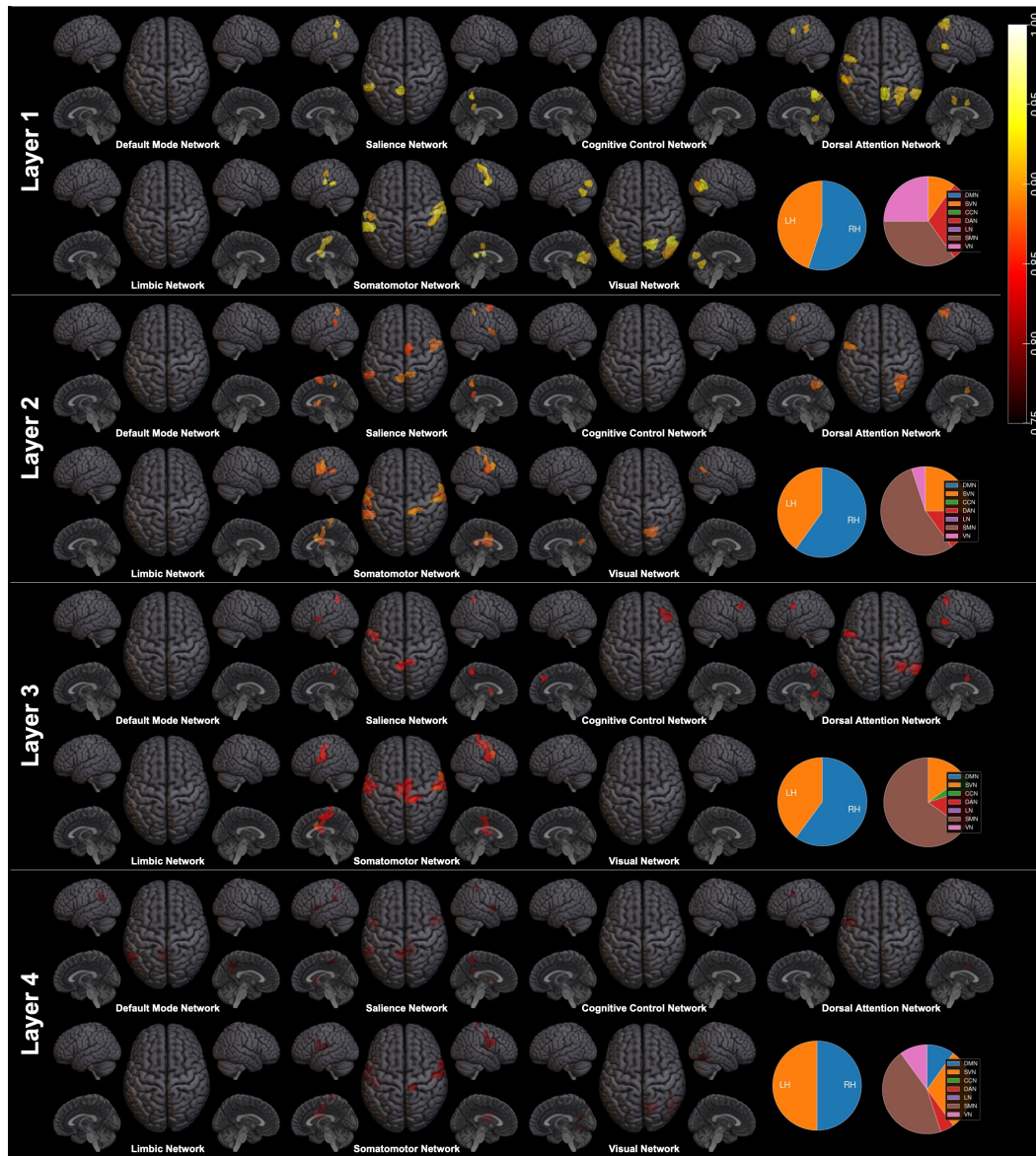


Figure 8: Brain plot of top 5-percentile HCP-Rest spatial attention regions.

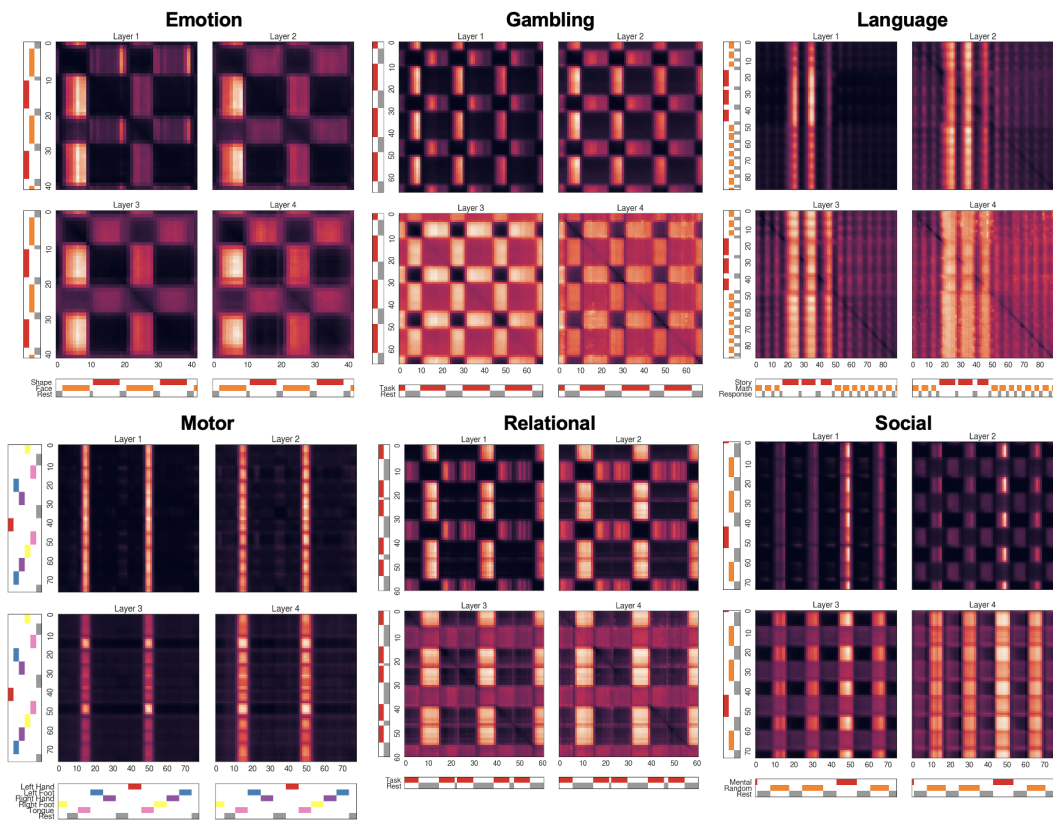


Figure 9: Plot of the HCP-Task temporal attention $Z_{\text{time}}^{(k)}$ averaged across all subjects.

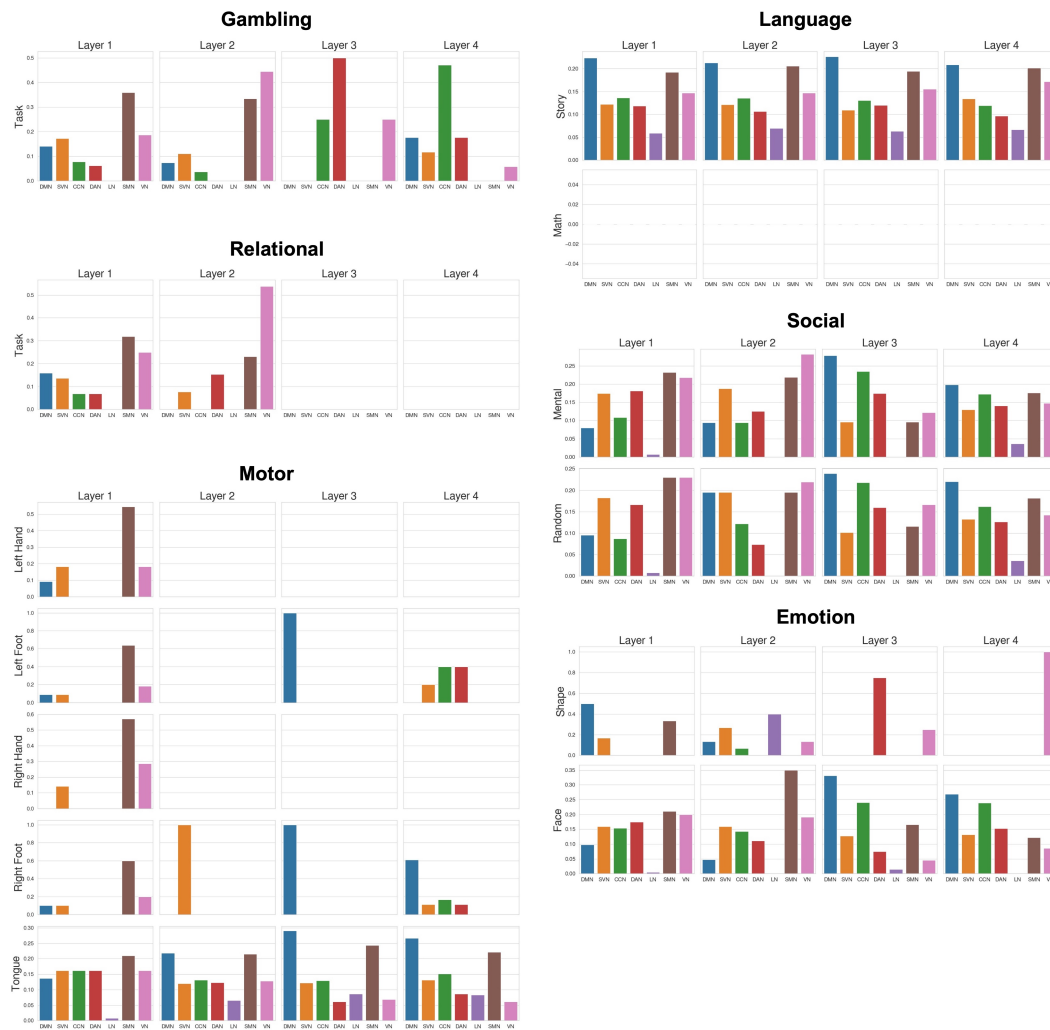


Figure 10: Proportion of statistically significant regions within the 7 ICNs from the HCP-Task spatial attention GLM. Each subtask is contrasted with the baseline subtask, i.e. rest or response.

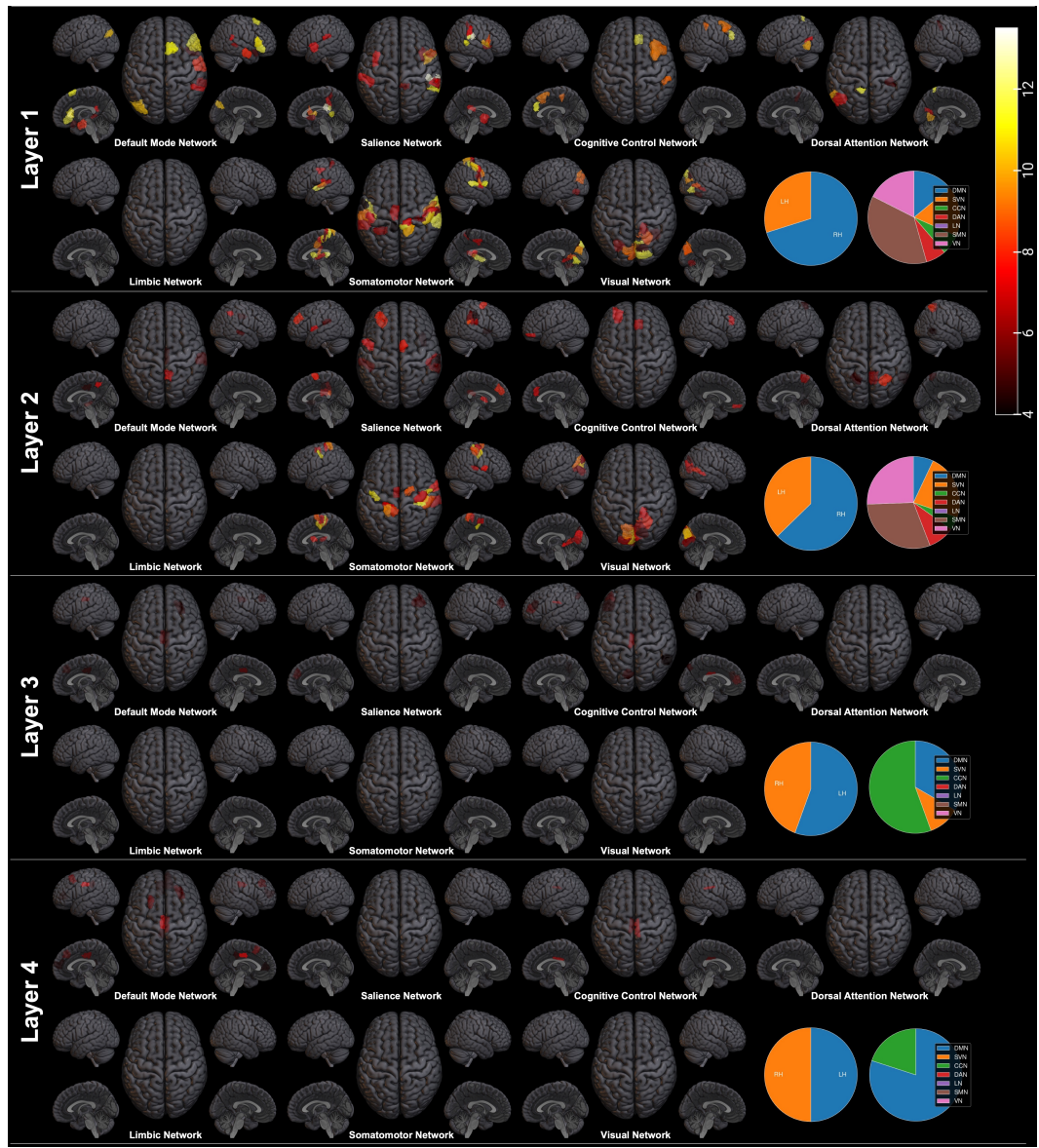


Figure 11: Brain plot of statistically significant HCP-Task working memory spatial attention regions.